

# NUMERICAL INVESTIGATION OF AIR JETS FOR DYNAMIC STALL CONTROL ON THE OA209 AIRFOIL

A.D. GARDNER\*, K. RICHTER† AND H. ROSEMAN‡

## ABSTRACT

The design and numerical investigation of constant blowing air jets as Fluidic Control Devices (FCDs) for helicopter dynamic stall control is described. Prospective control devices were first investigated using 3D RANS computations to identify effective configurations and reject ineffective configurations. Following this, URANS investigations on the dynamically pitching OA209 airfoil verified that configurations had been selected which reduced the peaks in pitching moment and drag while preserving at least the mean lift and drag from the clean wing. Two configurations using jets at 10% chord on the airfoil top were identified, and one configuration using a tangential slot at 10% chord on the airfoil top, with each configuration evaluated for two jet total pressures. For the best configuration, a reduction in the pitching moment peak of 85% and in the drag peak of 78% were observed, together with a 42% reduction in the mean drag over the unsteady pitching cycle.

## INTRODUCTION

The DLR-ONERA project SIMCOS is part of a long-term German-French cooperation to combat dynamic stall (DS) and improve numerical modelling with regards to dynamic stall. As part of this project the effect of pulsed and constant blowing jets on dynamic stall is being investigated both experimentally and numerically, with this paper describing the numerical investigation [7] for the design of a model for the Transonic Wind Tunnel Göttingen (DNW-TWG).

Dynamic stall is a well-known effect for many helicopter airfoils [15] occurring when a pitching airfoil stalls [2], forming separated flow in a dynamic stall vortex. A lift peak forms and then a rapid drop in lift and a negative spike in pitching moment appear as the stall vortex moves downstream. This torsional impulse is often a load-limiting case for the pitch links of the helicopter rotor blades, and high drag is experienced compared to attached flow. A device to combat dynamic stall will reduce the torsional impulse and drag, while improving the airfoil mean lift over a cycle.

The airfoil OA209 was chosen as a test object because it is an openly available contour [5] in use on a number of Eurocopter helicopters, for which good experimental databases from the DLR in the DNW-TWG and from ONERA in the F2 exist. It is an airfoil with thickness 9% chord,

which displays leading edge stall at Mach 0.3 and lower and displays a number of interesting dynamic stall behaviours [8, 12, 17]. The OA family of airfoils has been extensively investigated at the DLR with results for laminar separation bubble bursting [9] and for leading edge vortex generators for dynamic stall control [3, 13]. A predecessor study to this one [20] investigated the mesh densities and time step sizes necessary to get good CFD results for the clean OA209 airfoil, and test cases were identified where fully turbulent computations with a one-equation turbulence model gave good estimates of the airfoil performance when compared with experiment, including the test case used here.

Fluidic Control Devices (FCDs) have the advantage that, when turned off, the original airfoil contour and performance are available. Recent investigations into FCDs on an airfoil have often been performed with synthetic jet actuators (SJAs) in mind. These jets rely on a small plenum chamber behind a jet from which air is sucked in from the outside or ejected to the outside using a piston or diaphragm actuator. This type of jet has zero mass flux (ZMF) when integrated over a cycle, and thus only electrical power (no air) needs to be provided. Experiments using SJAs [24] show that the same results are achieved as with constant blowing, with an additional advantage which is attributed to the increased resistance of the boundary layer to separation due to the amplification of turbulent frequencies by the high frequency SJA injection. The same effect has also been noted for pulsed blowing from a high pressure source (not ZMF) [11]. The synthetic jet appears to be more efficient than constant blowing but the aerodynamic similarity between the two cases and the reduction in computational time by a factor 3-10 for the constant blowing over SJAs meant that constant blowing was selected to be studied.

Constant blowing or pulsed blowing at 1/cycle and up to 100/cycle at total pressures of up to 50 bar can be realised experimentally using valves [18] in the model installed behind each injection point. Turning off the blowing for a half-cycle will halve the air needed and pulsed blowing over a half cycle will further reduce the air needed by a factor of 2-3. Thus the constant blowing case is expected to define a lower limit of actuator effectiveness and an upper limit of air use. In this paper injection with supercritical jet conditions is described, where the gas expands to supersonic conditions after injection.

\*Corresponding Author. German Aerospace Center (DLR), Institute of Aerodynamics and Flow Technology (AS), Bunsenstrasse 10, 37073 Göttingen, Germany. [tony.gardner@dlr.de](mailto:tony.gardner@dlr.de)

†DLR-AS

‡DLR-AS

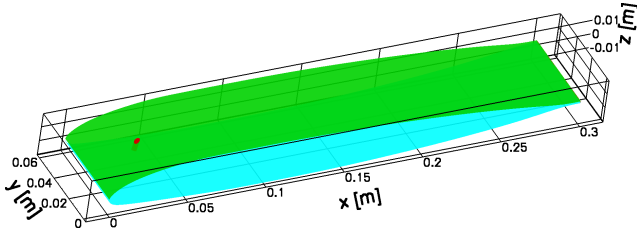


Figure 1: Airfoil gridded area.

## COMPUTATIONAL APPROACH

Computations using the DLR-TAU code are presented for a 3D slice of the dynamically pitching OA209 airfoil at the DS2 test condition:  $M=0.31$ ,  $Re=1.16e6$ ,  $\alpha=12.87\pm 7.13^\circ$ ,  $\omega^*(c)=0.101$ . Different types of air jets were investigated and evaluated for their ability to reduce the negative effects of dynamic stall, while preserving the positive effects. The values of pitching moment peak height and peak drag height were minimised, as was the mean drag. The mean lift and instantaneous lift at low angles of attack were maximised and high values were used an indicator of reduced lift hysteresis.

Reynolds-averaged Navier-Stokes (RANS) and Unsteady RANS (URANS) computations were undertaken with the DLR-TAU release 2009.1.0 [10, 21]. The node-based finite-volume solver was used on a hybrid unstructured grid consisting of prismatic layers close to the viscous surfaces and a tetrahedral field, generated using the Centaur<sup>TM</sup>[1] unstructured grid generator. All computations were fully turbulent, using the Spalart-Allmaras turbulence model [22] with the Edwards modification (SAE) [4], due to its excellent speed and stability, and the good results obtained for this test case by previous investigators. A central scheme was used with the scalar dissipation method of Mavriplis [14]. An LUSGS flux solver was used, with no multigrid convergence acceleration and a CFL number of 2.

The RANS computations used 10000 time-steps, for a total of around 60-80 CPUh, although true convergence was not reached due to the separated flow at the conditions computed. The coefficients were instead averaged over the last 2000 time steps to obtain the values quoted in this article. The URANS computations used 1600 time steps per period with 400 inner iterations per timestep. Significantly more inner iterations were required for convergence with jet injection than had been previously observed for clean cases. A minimum of 3 pitching cycles needed to be computed for convergence, with each cycle costing 3400-4400 CPUh.

The grid was generated according to the guidelines of Richter *et al* [20], with grid cells of 1% chord on the top and bottom of the airfoil and finer cells of 0.15% on the leading and trailing edges and around the jets. A 3D slice of the airfoil with a width of 20% chord (60 mm) was used. This was bounded by periodic side-walls (Figure 1) which allow a net spanwise flow for jet configurations with all jets skewed in one direction. The domain was selected to capture the qualitative effects required to make a good decision about which jet to choose, with a small number of node points (under 2 million) so that the geometry could be computed with acceptable cost by the URANS solver.

It is expected that this domain is insufficiently wide to see 3D effects for the main dynamic stall vortex, but the 3D

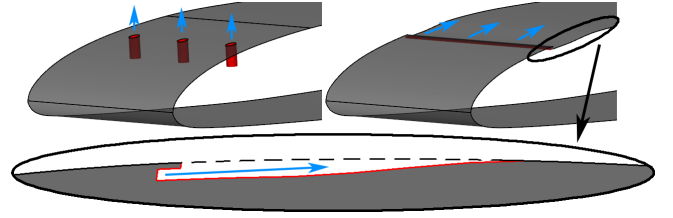


Figure 2: Comparison of airfoil modifications for portholes (left) and for tangential injection (right and bottom).

effects in the first 20-40% of the airfoil will be preserved, as needed for the jets. This type of computational domain has also been used by a number of other investigators, amongst them Prince *et al* [19], who got quite good results when compared with experiment for passive air-jet vortex generators in incompressible flow. In order for the effect of the jet boundary layer to be captured, the jets were modelled as short tubes sunk into the surface with a length of twice the jet diameter (or slot width), with a boundary setting the total temperature, pressure and density at the bottom end. In cases where a tangential slot of width 0.5 mm was to be used, the surface of the airfoil was changed, shifting the surface inward by 0.75 mm (to include the 0.25 mm wall outside the slot), and blending in all the changes back to the original contour within a length of 7% chord (Figure 2). The same method was used for all other tangential slots shown in this article.

## DEFINITIONS

**Reduced frequency:**  $\omega^* = \frac{2\pi fc}{v_\infty}$ , with  $f$  the oscillation frequency (Hz),  $c$  the chord and  $v_\infty$  the freestream velocity.

**Jet momentum ratio:**  $C_\mu = \frac{2}{bc} \frac{m_j v_j}{\rho_\infty v_\infty^2}$ , with  $m_j$  the mass flux out of the jets,  $v_j$  the jet speed at the jet exit (set to be a constant value,  $M=1.0$ ) and  $b$  the span width of the rotor blade.  $C_\mu$  is well-defined for the incompressible case ( $C_\mu = \frac{A}{c} \frac{v_j}{v_\infty}$ ), ( $A$  is the jet area), but its extension to compressible flow depends on the jet conditions used as a reference. The extension above is simplest, but differs from some definitions used in the literature.

**Jet mass ratio:**  $C_q = \frac{m_j}{\rho_\infty v_\infty cb}$ ,

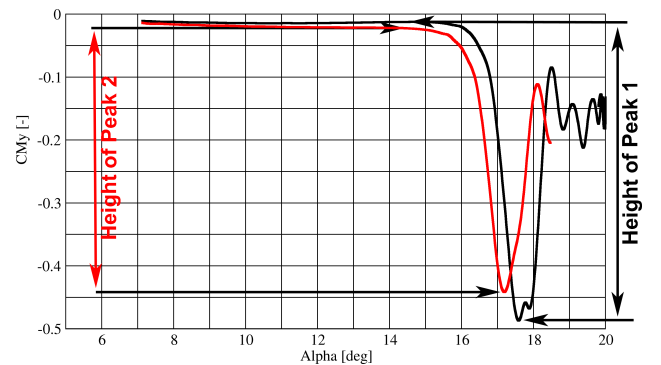


Figure 3: Measurement of the peak height for two sets of data.

**Drag and pitching moment peak heights:**  $CM_{y,p}$  and  $C_{D,p}$  are the difference between the value at the peak and “flat” value a short time beforehand (Figure 3).

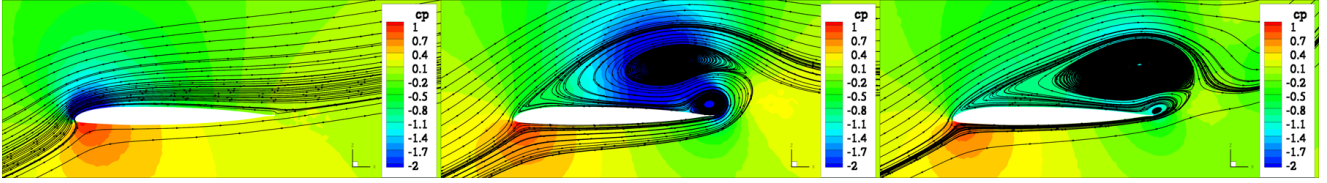


Figure 4: Comparison of flow topologies on the symmetry plane before (left), at (middle) and after (right) dynamic stall for the "Clean" OA209 airfoil.  $\alpha=15.6^\circ$ ,  $17.9^\circ$  and  $19.5^\circ$  respectively for an instantaneous solution at the periodic plane.

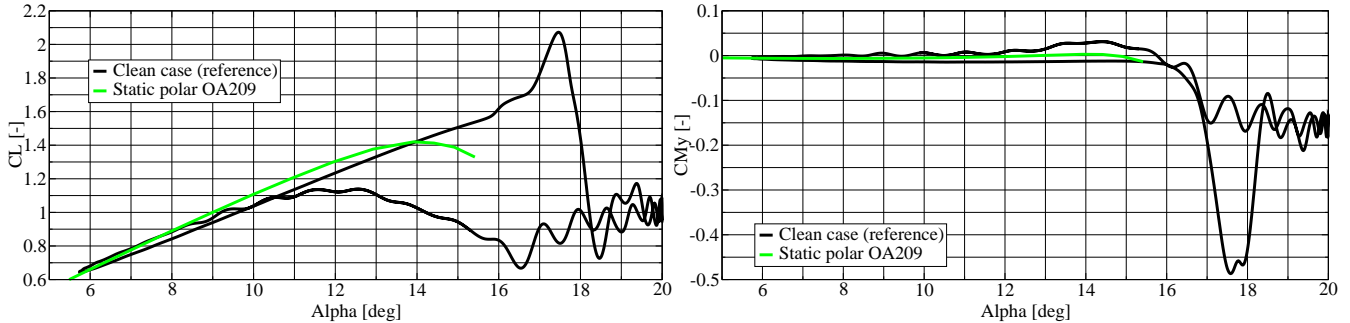


Figure 5: URANS results of the coefficients over one pitching cycle  $\alpha=12.87\pm 7.13^\circ$ ,  $\omega^*(c)=0.101$  for: (left) Lift coefficient, (right) Pitching moment coefficient. Shown is the result for the "Clean" OA209 airfoil compared with a static polar computed with RANS on a 2D grid with a farfield boundary.

**Mean values of lift and drag:**  $\overline{C_L}$  and  $\overline{C_D}$  are averaged over one pitching cycle.

**Mass flow:**  $\dot{m}_j$  is an output of the TAU solver for the jet boundaries. It is averaged over one pitching cycle and normalised to one meter of blade span width.

## DEEP DYNAMIC STALL ON THE OA209

The SIMCOS DS2 test case ( $M=0.31$ ,  $Re=1.16e6$ ,  $\alpha=12.87\pm 7.13^\circ$ ,  $\omega^*(c)=0.101$ ) shows all the typical behaviour of deep dynamic stall at low Mach numbers. At low angles of attack, on the upstroke, the flow is attached and is qualitatively similar to the statically attached flow (Figure 4, left). At stall, a large dynamic stall vortex appears, which is associated with a peak in the lift coefficient (Figure 4, middle). The vortex attachment point is at the nose and the large main vortex stretches to the leading edge with a counter-rotating vortex is formed from the trailing edge. After stall (Figure 4, right) the dynamic stall vortex moves downstream, and the pressure minimum in the center of the dynamic stall vortex wanders over the trailing edge of the airfoil, leading to a negative peak in the pitching moment. Additionally, the attachment point of the dynamic stall vortex (the separation point of the flow on the top of the airfoil) moves rearward, also increasing the pitching moment. The movement of the attachment point can be observed by the movement of the forward streamline of the dynamic stall vortex between Figures 4 (middle) and (right) but is difficult to see in these pictures. This negative peak in the pitching moment is the main undesirable effect of dynamic stall, and is the maximum load for the pitch links on a helicopter blade. The reduction in size and strength of the dynamic stall vortex is a central target of dynamic stall control strategies. In addition, better anchoring the attachment point of the dynamic stall vortex can reduce the height of the peak in the pitching moment.

Figure 5 shows the lift and pitching moment coefficients

over a cycle for the OA209 airfoil at the DS2 test condition. The upstroke has attached flow, before a peak in the lift coefficient associated with the formation of the main dynamic stall vortex (Figure 5, left). As the lift suddenly falls, a peak in the pitching moment coefficient is formed (Figure 5, right), which is associated with the movement of the dynamic stall vortex downstream, and with the downstream movement of the separation point. After stall there is unsteady, separated flow, which continues up to the maximum angle of attack and to around  $\alpha=16^\circ$  on the downstroke. This unsteady flow is caused by the shedding of smaller vortices from both the leading and trailing edges of the airfoil. After around  $\alpha=16^\circ$  on the downstroke the flow stabilises, and the flow reattaches, so that the bottom part of the downstroke again has flow qualitatively similar to the fully attached flow on a statically inclined airfoil.

The dynamic stall control strategies followed in this article will concentrate on using blowing with air jets to keep the flow attached, reduce the strength of the dynamic stall vortex, and to anchor the separation of the flow and the attachment point of the dynamic stall vortex. Each type of air jet used one or more of these types of flow control and, in the following sections, the air jets are grouped by the main type of flow control which they display. The strategies are:

1. Dynamic stall vortex reduction. Flow attachment was improved using air jets in the flow direction to push the separation point backward using the Coanda effect.
2. Coanda effect tangential blowing. The strength of the dynamic stall vortex was reduced by blowing across the airfoil to turn the dynamic stall vortex from a single vortex with only a y-component to its axis into one or more vortices with a vortex axis having components in the x, y, and z directions.
3. Limiting the separation vertical blowing. The dynamic stall vortex was stabilised by using vertical blowing from the surface to provide an anchor point for the separation and limit its upstream travel.

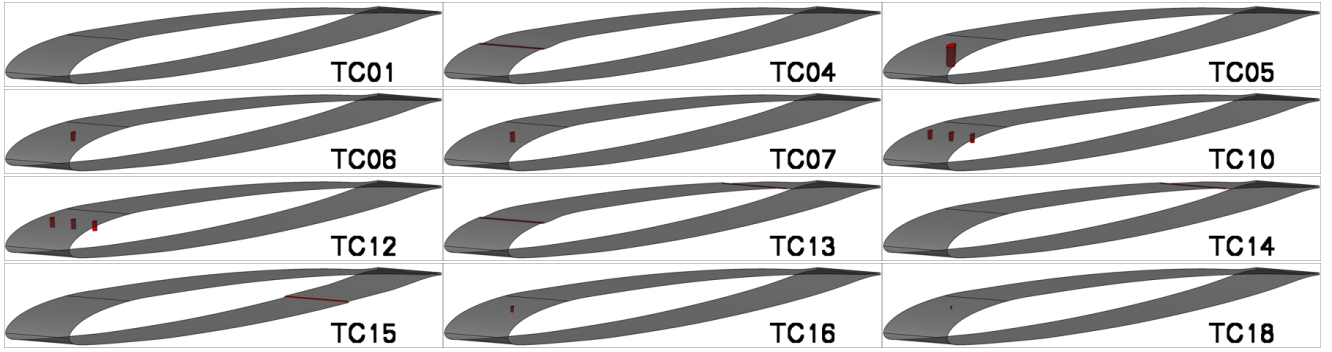


Figure 6: Test matrix of RANS computations.

## INITIAL INVESTIGATIONS

Initial investigations showed that approach of using URANS computations directly was too costly in both computing power and time to be used as the sole tool for the numerical investigation of these air jets. In contrast, RANS results above the static stall angle were found to be a relatively cheap method of identifying effective flow control devices. Thus potential flow control devices were first investigated with RANS before a reduced number of devices were investigated using URANS with full pitching motion.

It was found that the control of mass flow in low pressure jets was too unreliable, and instead supercritical configurations should be investigated. This meant that the impulse of the jet was significant and had to be taken into consideration. Finally, it was found that the jets should pierce the boundary layer without separating it, meaning that all configurations having slot injectors normal to the surface were removed from consideration because of the large separated regions which they caused.

## RANS RESULTS AT $\alpha=17.5^\circ$

Using RANS computations, 12 configurations (Figure 6) were investigated at  $M=0.31$ ,  $Re=1.16e6$  for a steady angle of attack of  $\alpha=17.5^\circ$ , well above the static stall angle of  $\alpha=14^\circ$  (Figure 5). This approach provided a qualitative estimate which jets would give a performance improvement over the clean case comparatively cheaply compared to URANS computations. The improvement in lift and drag compared with the reference airfoil identified interesting configurations, with only the three most interesting configurations extensively investigated using URANS on an airfoil with pitching motion. Each configuration was investigated for two air mass flow rates: a maximum flow rate of 0.22 kg/s per meter of blade and a flow of half that (0.11 kg/s/m), resulting in supercritical injection with pressure ratios across the jet of between 2 and 20. This approach simplified the local modelling of the jet since no feedback into the jet was expected and the main effect was of a macroscopic jet. The test cases are enumerated in Table 1 and Figure 6. An example for each grouping can be seen in Figure 7.

The test cases for the dynamic stall vortex vortex reduction use jets which were inclined at  $45^\circ$  downstream, and skewed at  $45^\circ$  across the flow with a jet spacing of 60 mm (for example TC06 in Figure 7) or 20 mm. In the RANS

Case	Jet Type ( $h/\phi$ )	Position	Space	Incline/ Skew
<b>Reference case</b>				
TC01	Clean OA209, width=60 mm, chord=300 mm			
<b>Dynamic stall vortex reduction</b>				
TC05	Hole (6 mm)	10% top	60 mm	$45^\circ/45^\circ$
TC06	Hole (3 mm)	10% top	60 mm	$45^\circ/45^\circ$
TC10	Hole (3 mm)	10% top	20 mm	$45^\circ/45^\circ$
TC16	Hole (2 mm)	10% top	60 mm	$45^\circ/45^\circ$
TC18	Hole (1 mm)	10% top	60 mm	$45^\circ/45^\circ$
<b>Coanda effect blowing</b>				
TC04	Slot (0.5 mm)	10% top	–	Tangent
TC13	Slot (0.5 mm)	10+75%t.	–	Tangent
TC14	Slot (0.5 mm)	75% top	–	Tangent
TC15	Slot (0.5 mm)	75% bot.	–	Tangent
<b>Dynamic stall vortex limitation</b>				
TC07	Hole (3 mm)	10% top	60 mm	Vertical
TC12	Hole (3 mm)	10% top	20 mm	Vertical

Table 1: Test cases.

results, three effects of the jets are observed: firstly a vortex is generated at the root of the jet, which propagates along the top side of the OA209, secondly a sideways momentum is given to the flow so that the dynamic stall vortex is not purely 2D, and finally the angling of the jets downstream reduces the drag, by adding some of the jet thrust in the forward direction, and turning the flow further toward the surface due to the Coanda effect. The vortex along the wall will help the flow to remain attached longer, and it is hoped that the break-up of the 2D vortex will reduce the height of the dynamic stall peaks in lift, drag and momentum as the dynamic stall vortex separates. It is postulated that a similar 3D effect due to model end conditions [6] causes the over-estimation of the size of the lift and pitching moment peaks at the moment that the dynamic stall vortex separates when compared with experiment [20].

The jet diameter and spacing were varied at constant mass flow for the dynamic stall vortex vortex reduction. With reducing hole diameter and constant mass flow through the jets, smaller jets have higher Mach number, stagnation pressure and injected energy (Table 2). The overall effect of reducing the spacing to 20 mm is a reduction in lift and an increase in drag over the single jet case, since the flow is not turned as much toward the airfoil, and no vortices are created along the top surface of the airfoil. In fact the total effect of reducing the spacing to 20 mm (TC10) is to join the

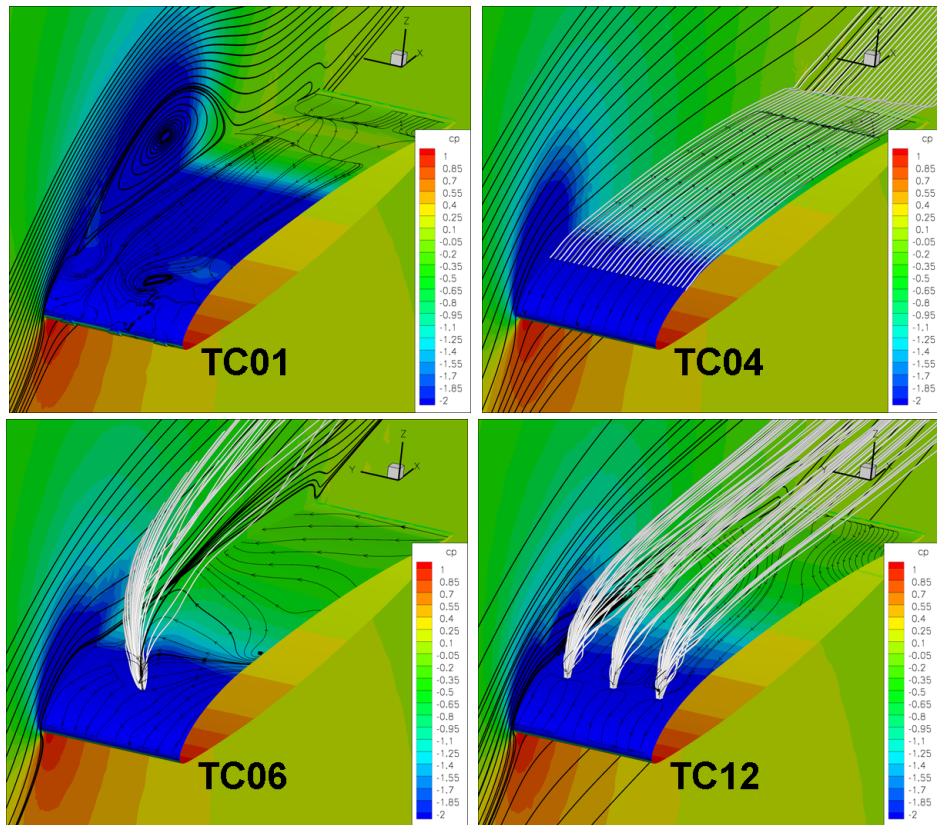


Figure 7: Test matrix for URANS computations with an example of each jet type group, showing flow state at  $\alpha=16.35^\circ$  on the upstroke for the maximum mass flow rate tested. (Top, left) Clean case with unsuppressed DS vortex (TC01); (Top, right) tangential slot 0.5 mm (TC04); (Bottom, left) 3 mm jet at 60 mm spacing inclined/skewed at  $45^\circ/45^\circ$  (TC06); (Bottom, right) Vertical 3 mm jet at 20 mm spacing (TC12). Jets were at 10% chord.

jet flows into a single blockage. As seen in Table 2, all of the 60 mm jet spacing configurations increased lift by 50-80%, and decreased drag by around 35%. The TC06 was selected for URANS testing due to practical considerations of the feeder pressure and geometry.

The test cases for the Coanda effect blowing use slots tangential to the airfoil surface to increase lift by turning the external flow back toward the airfoil (for example TC04 in Figure 7). This is done by using the Coanda effect on the flow near the separation streamline, and by providing blowing in the streamwise direction along the wall so that the reverse flow, which would form near the airfoil for separated flow, is not permitted. Slot blowing at the 10% chord position caused fully attached flow on the rear 90% of the airfoil, and only a small separation of the front 10% of the airfoil. As seen in Table 2, for the TC04 the lift is increased by 70% and the drag is reduced by 60%, due in part to the direction of the jet rearward, and also to the almost complete absence of separated regions.

Two basic problems remain with the tangential slot jets. Firstly due to the large exit area of the slots the jet pressures used are low, leaving little room to operate at lower pressure for reduced effect, and the possibility of reducing the slot width is limited since the slot is already only 0.5 mm wide. Additionally the alteration of the airfoil contour at the point where the highest Mach number flow is found on the advancing blade is likely to be a serious problem unless the slot itself is a deployable object. The TC04 was nevertheless selected for URANS testing because of its good performance.

The test cases for the dynamic stall vortex limitation use vertical jets at 10% chord to limit the upstream travel of the dynamic stall vortex (similarly to the back-flow flap [16, 23]), and convert it to a static separation, with accompanying suppression of dynamic separation effects (for example TC12 in Figure 7). The idea is to create a separation limiting effect similar to that possible for a vertical slot, but without forcing the boundary layer to separate fully.

This idea did not work fully for a jet spacing of 60 mm. However with a jet spacing of 20 mm (TC12) the size of the separation is limited by the front edge of the separation anchoring at the jet, and a modest improvement in lift, drag and pitching moment were achieved, with around 30% improvement in lift and 30% reduction in drag over the reference case, as can be seen in Table 2. Confirming the selection of TC12 for further URANS study were the results at half pressure, where the flow was fully turned and only a small separation was seen behind the jets. It is postulated that the additional ventilation provided to the back half of the airfoil between the jets causes the large difference to the vertical slot case investigated initially. For the half-pressure case, the improvement in lift over the reference case was only 20%, but the drag was only 60% of that for the reference case, and improvement of 10% over the case with full pressure.

The RANS computations indicated a reduction in drag and an increase in lift for configurations with air jets which allowed the configurations using each of the three control strategies to be identified. As an example of the Coanda effect blowing, the tangential slot configuration TC04 was

Case Name	$P_{0j}$ (bar)	$\dot{m}_j$ (kg/s/m)	$C_L$ /Ref	$C_D$ /Ref	$CM_{y_p}$ /Ref
<b>Reference case</b>					
TC01	0	0	1.00	1.00	1.00
<b>DS vortex reduction (<math>C_q=0.01, C_\mu=0.06</math>)</b>					
TC05	3.04	-0.22	1.52	0.64	0.28
TC06	11.11	-0.22	1.72	0.66	0.27
TC10	3.35	-0.22	1.24	0.99	1.20
TC16	41.68	-0.22	1.72	0.62	0.23
TC18	278.9	-0.22	1.79	0.63	0.22
<b>DS vortex reduction (<math>C_q=0.005, C_\mu=0.03</math>)</b>					
TC05	1.52	-0.12	1.02	0.93	0.90
TC06	5.55	-0.11	1.01	0.94	0.89
TC10	1.67	-0.11	0.94	0.88	0.81
TC16	20.84	-0.12	1.14	0.85	0.72
TC18	120.2	-0.11	0.97	0.96	1.01
<b>Coanda effect blowing (<math>C_q=0.01, C_\mu=0.06</math>)</b>					
TC04	2.07	-0.22	1.70	0.39	-0.01
TC13	1.04	-0.22	1.01	0.64	0.54
TC14	1.99	-0.22	1.08	0.92	1.14
TC15	1.99	-0.22	1.09	0.90	1.14
<b>Coanda effect blowing (<math>C_q=0.005, C_\mu=0.03</math>)</b>					
TC04	1.03	-0.11	0.86	0.74	0.56
TC13	0.52	0.01	1.05	0.87	0.79
TC14	1.00	-0.11	0.97	0.95	0.94
TC15	1.00	-0.11	1.03	0.95	0.95
<b>DS vortex limitation (<math>C_q=0.01, C_\mu=0.06</math>)</b>					
TC07	24.40	-0.22	0.94	0.80	0.94
TC12	6.70	-0.22	1.31	0.73	0.59
<b>DS vortex limitation (<math>C_q=0.005, C_\mu=0.03</math>)</b>					
TC07	12.20	-0.12	0.92	0.97	0.99
TC12	3.35	-0.12	1.23	0.59	0.10

Table 2: Results of the RANS investigations.

selected. As an example of the dynamic stall vortex reduction, the inclined/skewed jet configuration TC06 was selected. As an example of the dynamic stall vortex limitation and anchoring the vertical jet configuration TC12 was selected. These configurations were then investigated using URANS computations with pitching motion.

## URANS RESULTS WITH $\alpha=12.87\pm 7.13^\circ$

The test cases TC01, TC04, TC06 and TC12 were investigated with URANS computations on a dynamically pitching OA209 airfoil. The test cases are shown in Figure 7 and have one example of each flow control method, together with the reference case. The images in Figure 7 are all taken at  $\alpha=16.35^\circ$  on the upstroke, and large differences in the flow topology due to the flow control mechanisms are visible. The flow in the reference case has just developed the main dynamic stall vortex, where the cases with air blowing have all suppressed it to some degree. For the TC04, which used blowing from a slot parallel to the airfoil surface, the flow is fully attached except for a small, flat separation near the trailing edge. For the TC06, which used jets inclined in the flow direction and skewed to the left, the separation has been greatly reduced, and no real vortex is currently visible.

Case Name	$P_{0j}$ (bar)	$\dot{m}_j$ (kg /s/m)	$\bar{C}_L$ /Ref	$\bar{C}_D$ /Ref	$CM_{y_p}$ /Ref	$C_{D_p}$ /Ref
<b>Reference case</b>						
TC01	0	0	1.00	1.00	1.00	1.00
<b>DS vortex reduction (<math>C_q=0.01, C_\mu=0.06</math>)</b>						
TC06	11.11	-0.22	1.07	0.56	0.74	0.68
<b>DS vortex reduction (<math>C_q=0.005, C_\mu=0.03</math>)</b>						
TC06	5.55	-0.11	1.03	0.73	0.76	0.79
<b>Coanda effect blowing (<math>C_q=0.01, C_\mu=0.06</math>)</b>						
TC04	2.07	-0.22	1.18	0.31	0.62	0.62
<b>Coanda effect blowing (<math>C_q=0.005, C_\mu=0.03</math>)</b>						
TC04	1.03	-0.11	1.07	0.68	0.83	0.80
<b>DS vortex limitation (<math>C_q=0.01, C_\mu=0.06</math>)</b>						
TC12	6.70	-0.22	0.99	0.58	0.15	0.22
<b>DS vortex limitation (<math>C_q=0.005, C_\mu=0.03</math>)</b>						
TC12	3.35	-0.12	1.02	0.61	0.29	0.31

Table 3: Results of the URANS investigations.

A strong sideward component to the flow on the surface as been created due to the jet skew. For the TC12, which used vertical jets, the flow is separated both before and after the jets, but the size of both is reduced. A strong anchoring of the separation on the back of the airfoil at the position of the jets is visible, as is the termination of the separated region on the front of the airfoil by the jets.

*Coanda effect blowing:* The effect of the 0.5 mm slot used for the Coanda effect blowing test case (TC04) is to shift the separation vortex rearward and cause earlier reattachment (Figure 8). The high Mach number of the air exiting the slot causes a small separation in front of the slot during the upstroke (Figure 8, left), which expands as the angle of attack increases, but is qualitatively similar, even after stall. After stall, the blowing prevents the formation of the dynamic stall vortex until halfway back on the airfoil (Figure 8, middle). This vortex is smaller, weaker and positioned further back than for the clean case, meaning that the lift and pitching peaks are reduced. As the dynamic stall vortex becomes very large and moves over the trailing edge of the airfoil (Figure 8, right) the blowing of the jet still enforces attached flow along the majority of the airfoil.

The stall for the TC04 occurs at approximately the same angle as for the reference airfoil, and there is no large lift peak since no large dynamic stall vortex forms (Figure 9, left). An increase in lift of up to 15% was seen during the attached flow part of the upstroke due to the jet being pointed directly aft of the airfoil, decreasing at lower angles of attack, and a net thrust (negative drag) was produced at low angles of attack. While the improvements in mean lift (18%) and mean drag (69%) are impressive (Table 3) they come at the cost of a significant modification to the airfoil contour for the injection slot and the creation of a second dynamic stall vortex. The pitching moment peak from the first DS vortex is reduced by 38% (Figure 9, right) and the shape of both the lift and pitching moment peaks is rounded when compared to the reference case. The rounding of the lift peak is due to the slow growing of a separation on the front part of the airfoil, which is prevented by the jet from spreading backwards as is the case for the clean airfoil. In addition, the growth of the main dynamic stall vortex limited to the back half of the airfoil. The vortex later swims off,

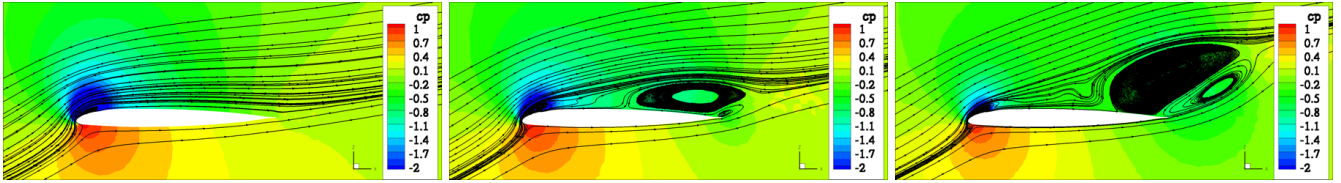


Figure 8: Comparison of flow topologies on the symmetry plane before (left), at (middle) and after (right) dynamic stall for the "TC04" (tangential slot blowing) OA209 airfoil.  $\alpha=16.4^\circ$ ,  $17.5^\circ$  and  $18.5^\circ$  respectively for an instantaneous solution at the periodic plane (between the jets).

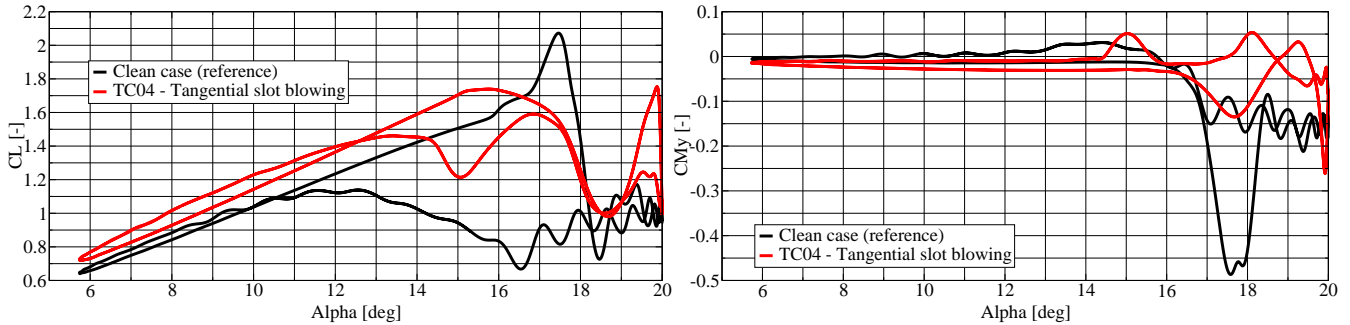


Figure 9: URANS results of the coefficients over one pitching cycle  $\alpha=12.87\pm 7.13^\circ$ ,  $\omega^*(c)=0.101$  for: (left) Lift coefficient, (right) Pitching moment coefficient. Shown is the result for the "TC04" (tangential slot blowing) plotted against the "Clean" OA209 airfoil.

but without giving a large dynamic stall peak. The RANS results for TC04 (Table 2) suggest that the lift should be increased by 70% and the drag reduced by 60%, but this is not the case for any angle in the upstroke, but a 75% increase in lift and 60% decrease in drag can be seen on the downstroke at around  $17^\circ$ . Due to the airfoil modification, the TC04 is not preferred to the porthole configurations TC06 or TC12.

*Dynamic stall vortex reduction:* The effect of the inclined and skewed jets (TC06) is to reduce the size of the dynamic stall vortex and to stabilise its position at the jets. Figure 10 (left) shows the flow on the symmetry plane, just after the end of the attached flow section of the upstroke. Here the sideways flow of the air jets causes a stable deviation of the streamlines upward away from the trailing edge of the airfoil which does not immediately separate. Instead this state persists for around  $\Delta\alpha=3^\circ$  until finally a dynamic stall vortex starts to form, at a delay of about  $\Delta\alpha=2^\circ$  from the reference case (Figure 10, middle). Finally the dynamic stall vortex moves downstream (Figure 10, right), with a considerably reduced strength, but the counter-rotating vortex formed at the trailing edge is much stronger. As a result of the strengthening of the counter-rotating vortex, a second dynamic stall vortex is produced, which is as strong as the original vortex.

With TC06 a constant lift up to just over  $\alpha=19^\circ$  (Figure 11, left) is produced, and the lift peak seen in the reference case does not appear. After separation and on the downstroke a second vortex is released from the surface creating a second peak not present in the clean case. The two peaks in the pitching moment are equally large (Figure 11, right) and are reduced by 26% over the clean case. The first peak in pitching moment is moved around  $2^\circ$  higher in angle, consistent with movement seen in the drop in lift coefficient. Likewise the peak in drag (Table 3) is reduced by 32%, with a similar movement in the peak position. After this the flow in the reference and TC06 test cases is rather similar, although the reattachment for the TC06 is

marginally later. For the test case DS2 investigated here, dynamic stall could not be avoided, but indications are that for light dynamic stall the separation may be delayed sufficiently to avoid dynamic stall entirely.

As seen in Table 3, the improvements in the mean lift and drag for TC06 were 7% and 44% respectively, compared with the 70% and 34% predicted by the RANS computations. Some of this is because the RANS computations only look at the flow above stall, but it is clear that the RANS computations are a qualitative indication rather than a quantitative predictor.

Due to the narrowness of the computational domain (20% chord), the splitting of the main dynamic stall vortex into smaller vortices with x, y and z components to the axis was not captured. It is expected that these vortices would have a width of around 1 chord and so a computational domain of at least 2-3 chords would be needed to capture this behaviour, for a computational cost around 10 times that of these investigations. Additionally, due to the computational domain size a quasi-two-dimensionality is enforced at the trailing edge which will tend to strengthen both the dynamic stall vortex and the counter-rotating vortex from the trailing edge, so it remains to be seen whether a full 3D investigation can better estimate the respective strengths of these two vortices. This effect would be expected to further reduce the strength of the dynamic stall vortex.

*Dynamic stall vortex limitation:* The effect of the vertical jets for dynamic stall vortex limitation (TC12) is to cause the formation of a static separation bubble behind the injection position, which is stable in size and anchored in position by the jets. This separation is limited in height and does not block the flow. A separation is also formed in front of the jets, but this is stable and not connected to any other separation region. As seen in Figure 12 (left), the vertical blowing is detrimental during the parts of the cycle with attached flow, since it forces the flow before and after the jets to separate, as well as reducing the lift due to the direct

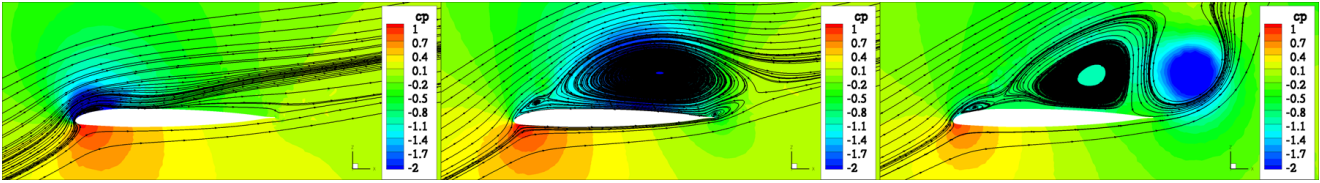


Figure 10: Comparison of flow topologies on the symmetry plane before (left), at (middle) and after (right) dynamic stall for the "TC06" (inclined/skewed blowing) OA209 airfoil.  $\alpha=16.4^\circ$ ,  $19.2^\circ$  and  $19.7^\circ$  respectively for an instantaneous solution at the periodic plane (between the jets).

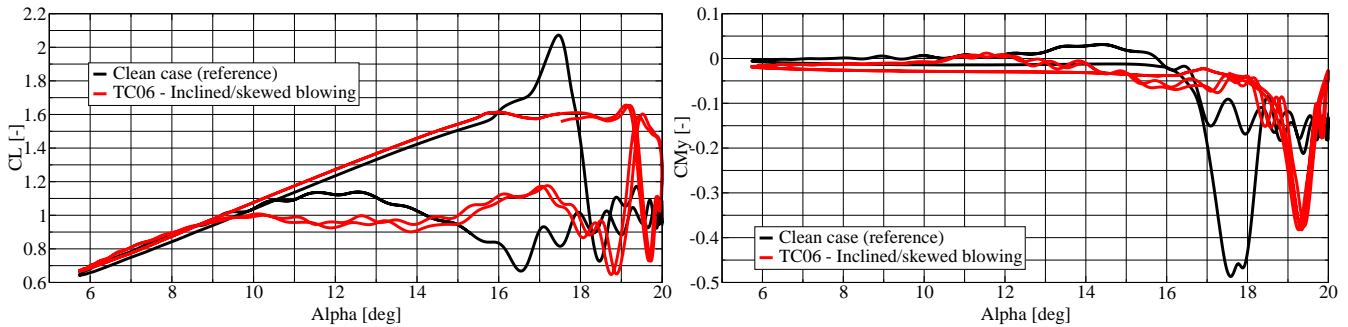


Figure 11: URANS results of the coefficients over one pitching cycle  $\alpha=12.87 \pm 7.13^\circ$ ,  $\omega^*(c)=0.101$  for: (left) Lift coefficient, (right) Pitching moment coefficient. Shown is the result for the "TC06" (inclined/skewed blowing) plotted against the "Clean" OA209 airfoil.

jet acceleration downward on the airfoil. In a practical implementation with constant blowing the jets would only be turned on during the parts of the cycle needing stabilisation, so this is not necessarily a problem. Switching the flow on and off once each per cycle was investigated numerically, and it could be shown that at the start and end of jet actuation the solution moved neatly between the solution for the jets and the solution for the clean OA209 airfoil in under  $\Delta\alpha=0.5^\circ$  of movement.

At stall (Figure 12, middle), a dynamic stall vortex similar to that seen for TC04 is formed near the rear of the airfoil. In addition a long, flat separation lying close to the airfoil surface stretches between the jets and the upstream side of the dynamic stall vortex. After stall (Figure 12, right) the flat separations around the injectors stretch to the trailing edge and this causes the flow to be less unstable than for the reference case, even though separation is present. A similar arrangement using a vertical slot produces an unstable separated region, and the stabilising effect in this case is the ventilation of the separated region from the front between the individual jets.

As seen in Figure 13 (left) the separation of the flow occurs at about the same angle of attack as for the reference airfoil ( $\alpha=16^\circ$ ), but the stabilisation of the separation results in a much more stable coefficient history after separation. The lift near the maximum angle is improved by 20% between  $\alpha=19^\circ$ - $20^\circ$ , somewhat less than the 31% gain predicted by the RANS computations. The flow reattaches around  $\Delta\alpha=3^\circ$  later than for the reference case, meaning that the mean lift was reduced 1% from the reference case (Table 3), although when only the top half of the cycle is considered, a modest 5% gain over the reference case is seen. The late reattachment can be solved by turning the jets off at the appropriate moment.

The improvement in the pitching moment coefficient (Figure 13, right) is by far the best for any configuration investigated, and no second dynamic stall peak is formed.

As reported in Table 3, a reduction in the pitching moment peak of 85% was found and the mean drag coefficient is improved by 42%, much better than the 27% predicted by the RANS computations.

## BLOWING WITH REDUCED PRESSURE

To investigate whether the improvements noted in mean lift, mean drag, pitching moment peak and drag peak were linear with the amount of air used for blowing, each of the test cases TC04, TC06 and TC12 were also tested with half the blowing pressure above. For TC04 (tangential slot blowing) and TC06 (inclined/skewed blowing), the effect of the pressure reduction was to create a qualitatively similar change to that for the full pressure case, but with the improvements in mean lift, mean drag, pitching moment peak and drag peak over the reference case approximately halved (Table 3). This means that the improvements will react linearly. For TC04, the pressure was reduced to around 1 bar, which was the limit for supersonic blowing in this case, which sets the lower limit for this linear relationship. For TC06 a further factor of 5.5 reduction in pressure would be possible before the pressure is at 1 bar and the blowing is no longer supersonic.

For the vertical blowing (TC12), halving the blowing pressure had less effect than expected by a linear dependency. As seen in Table 3, the mean lift and drag were marginally improved, mostly due to the reduction of the negative effects of the vertical blowing, since the jet effect downward and the size of the separation around the jets in the attached flow are both reduced (Figure 14, left). As the dynamic stall vortex forms (Figure 14, middle), the size is approximately the same as for the full-pressure case, but the separations around the jet are flatter and closer to the body. The dynamic stall vortex remains attached to the airfoil longer than for the full-pressure case (Figure 14, right).

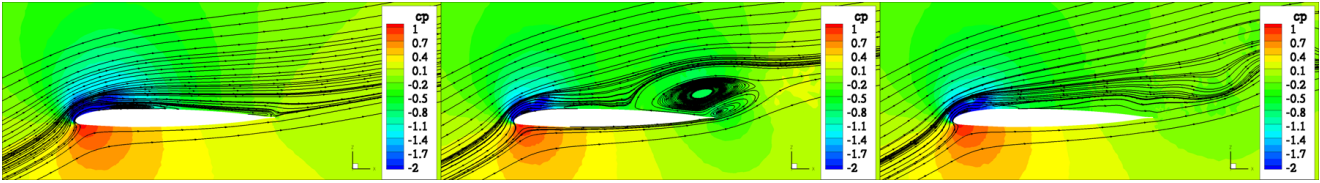


Figure 12: Comparison of flow topologies on the symmetry plane before (left), at (middle) and after (right) dynamic stall for the "TC12" (vertical blowing) OA209 airfoil.  $\alpha=16.4^\circ$ ,  $17.5^\circ$  and  $18.5^\circ$  respectively for an instantaneous solution at the periodic plane (between the jets).

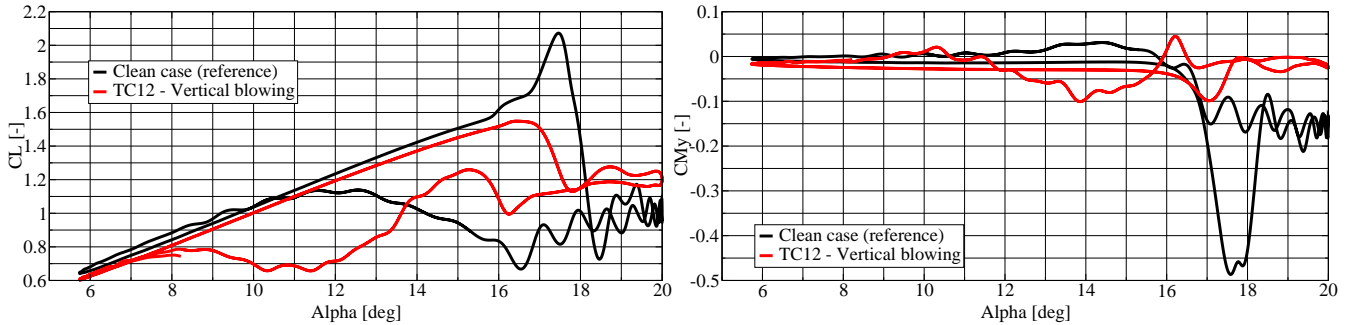


Figure 13: URANS results of the coefficients over one pitching cycle  $\alpha=12.87\pm 7.13^\circ$ ,  $\omega^*(c)=0.101$  for: (left) Lift coefficient, (right) Pitching moment coefficient. Shown is the result for the "TC12" (vertical blowing) plotted against the "Clean" OA209 airfoil.

The improvement in the behaviour during the attached flow can be seen in the history of the lift coefficient (Figure 15, left) where the lift is now approximately the same as for the reference case. In addition the reduced pressure allows earlier reattachment of the flow during the downstroke. The reduction to the pitching moment peak was still 71% over the reference case, rather than 42% as might be linearly expected (Table 3) and it can be seen that the pitching moment history is qualitatively similar to that for the full-pressure blowing (Figure 15, right).

## CONCLUSION

The numerical investigation of air jets for dynamic stall control has been described for the SIMCOS DS2 test case ( $M=0.31$ ,  $Re=1.16e6$ ,  $\alpha=12.87\pm 7.13^\circ$ ,  $\omega^*(c)=0.101$ ). The dynamic stall control strategies concentrated on using blowing with air jets to keep the flow attached, reduce the strength of the dynamic stall vortex, and to anchor the separation of the flow and the attachment point of the dynamic stall vortex. Steady RANS computations were first used to narrow a wide field of candidates to one candidate for each flow control strategy.

Computations using URANS on the pitching airfoil showed that each of the three candidates investigated increased the mean lift and reduced the mean drag over a pitching cycle, while reducing the peaks in pitching moment and drag caused during the production of the dynamic stall vortex. Each configuration was investigated for two blowing pressures to investigate the linearity of the flow control effect. From the results of the URANS computations, a configuration using vertical 3 mm portholes at 10% chord and 20 mm spacing (TC12) is the preferred configuration, with a configuration using a 3 mm inclined porthole at 60 mm spacing (TC06) as a second choice and a tangential slot (TC04) as the third choice. For the best configuration

(TC12), improvements in the pitching moment peak of 85% and in the drag peak of 78% were observed, together with a 42% reduction in the mean drag over the unsteady pitching cycle. Based on these results a wind tunnel model for the DNW-TWG is being constructed to investigate pulsed blowing on the vertical jet configuration, with the expectation that a control of the dynamic stall peak can be achieved using less air power than that saved in the airfoil drag.

The vertical jets have the interesting property of stabilising the separation point at the point of injection, with a small separation in front of the jets which stabilises the large vortex behind the jets by a constant flow between the jets. This avoids the unsteadiness in attachment position and size of the large vortex which would otherwise appear, such that the flow after separation is less unsteady than without flow control.

An open question from this investigation is the effect of a 3D computation with sufficient domain width to see full 3D development of the stall vortex, since the domain width here was so narrow as to enforce mainly 2D behaviour at higher stall angles.

## REFERENCES

- [1] [www.centaursoft.com](http://www.centaursoft.com)
- [2] Chandrasekhara, M.S., Wilder, M.C., Carr, L.W., *Competing Mechanisms of Compressible Dynamic Stall*, AIAA Journal, Vol. 36, No. 3, pp387-393, 1998.
- [3] Dietz, G., Mai, H., Geissler, W., *Auftriebsfläche mit verbessertem Ablöseverhalten bei stark veränderlichem Anstellwinkel*, European Patent EP 1 714 869 A1, 25.10.2006.
- [4] Edwards, J.R., Chandra, S., *Comparison of Eddy Viscosity-Transport Turbulence Models for Three-Dimensional, Shock-Separated Flowfields*, AIAA Journal, Vol. 34, No. 4, April 1996.

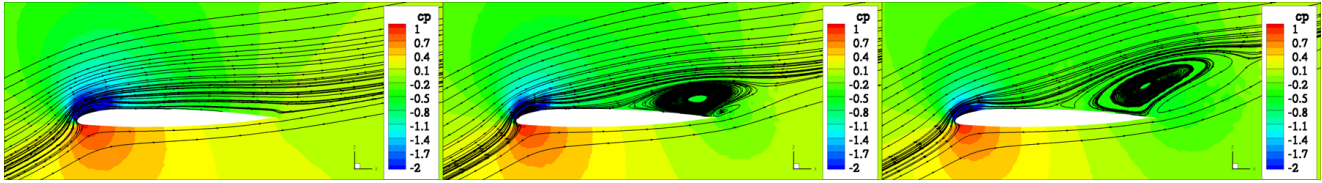


Figure 14: Comparison of flow topologies on the symmetry plane before (left), at (middle) and after (right) dynamic stall for the "TC12" (vertical blowing) OA209 airfoil at half pressure.  $\alpha=16.4^\circ$ ,  $17.5^\circ$  and  $18.5^\circ$  respectively for an instantaneous solution at the periodic plane (between the jets).

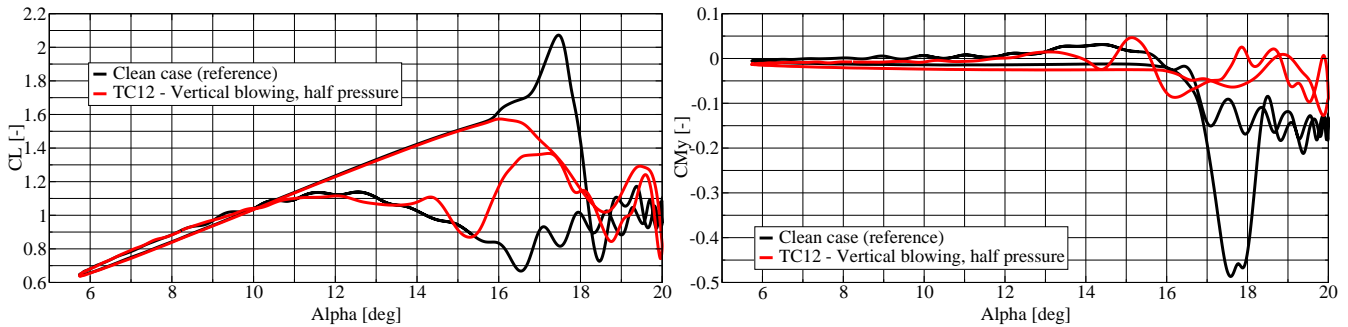


Figure 15: URANS results of the coefficients over one pitching cycle  $\alpha=12.87 \pm 7.13^\circ$ ,  $\omega^*(c)=0.101$  for: (left) Lift coefficient, (right) Pitching moment coefficient. Shown is the result for the "TC12" (vertical blowing) with half-pressure blowing plotted against the "Clean" OA209 airfoil.

- [5] Gallot, J., Vingut, G., De Paul, M. V., Thibert, J., *Blade profile for rotary wing of an aircraft*, United States Patent 4325675, April 20 1982.
- [6] Gardner, A.D., Richter, K., Rosemann, H., *Prediction of the Wind Tunnel Sidewall Effect for the iGREEN Wing-Tailplane Interference Experiment*, STAB2008, Aachen, 2008.
- [7] Gardner, A.D., *Numerical investigation of air jets for dynamic stall control on the OA209 airfoil*, DLR-IB 224-2009 A32, 2009.
- [8] Geissler, W., Dietz, G., Mai, H., Bosbach, J., Richard, H., *Dynamic Stall and its Passive Control Investigations on the OA209 Airfoil Section*, In: 31th European Rotorcraft Forum, Florence, Italy, 2005.
- [9] Geissler, W., Haselmeyer, H., *Investigation of Dynamic Stall On-Set*, Aerospace Science and Technology, Elsevier Masson SAS, pp590-600, 2006.
- [10] Gerhold, T., Friedrich, O., Evans, J. and Galle, M., *Calculation of Complex Three-Dimensional Configurations Employing the DLR-TAU-Code* AIAA-paper 97-0167, 1997.
- [11] Greenblatt, D., Wyganski, I., *Dynamic Stall Control by Periodic Excitation, Part 1: NACA0015 Parametric study*, Journal of Aircraft, V38 N3, pp430-447, 2001.
- [12] Heine, B., Mulleners, K., Gardner, A., Mai, H., *On the effects of leading edge vortex generators on an OA209 airfoil*, ODAS2009, 2009.
- [13] Mai, H., Dietz, G., Geissler, W., Richter, K., Bosbach, J., Richard, H., de Groot, K., *Dynamic stall control by leading edge vortex generators*, Journal of the American Helicopter Society, 53 (1). pp. 26-36, 2008.
- [14] Mavriplis, D.J., Jameson, A., Martinelli, L., *Multigrid solution of the Navier-Stokes Equations on triangular Meshes*, ICASE-report No. 89-35, 1989.
- [15] McCroskey, M.C., McAlister, K.W., Carr, L.W., Pucci, S.L., *An Experimental Study of Dynamic Stall on Advanced Airfoil Sections Volume 1. Summary of the Experiment*, NACA-TM 84245 1982.
- [16] Meyer, R.K.J., *Experimentelle Untersuchungen von Rückstromklappen auf Tragflügeln zur Beeinflussung von Strömungsablösungen*, Dissertation, Technische Universität Berlin, FB10, 2000.
- [17] Mulleners, K., Henning, A., Mai, A., Raffel, M., Le Pape, A., Costes, M., *Investigation of the Unsteady Flow Development over a Pitching Airfoil by Means of TR-PIV*, AIAA 2009-3504, 2009.
- [18] Neuhaus, D., *Magnetisch betätigbares Ventil*, Deutsches Patent DE 10 2005 035 878, 31.8.2006.
- [19] Prince, S.A., Khodagolian, V., Singh, C., *Aerodynamic Stall Suppression on Airfoil Sections Using Passive Air-Jet Vortex Generators*, AIAA Journal, Vol. 47, No. 9, pp2232-2242, 2009.
- [20] Richter, K., Le Pape, A., Knopp, T., Costes, M., Gleize, V., Gardner, A.D., *Improved Two-Dimensional Dynamic Stall Prediction with Structured and Hybrid Numerical Methods*, 65th AHS Forum, Grapevine (Texas), 2009.
- [21] Schwamborn, D., Gardner, A., von Geyr, H., Krumbein, A., Lüdeke, H., Stürmer, A., *Development of the TAU-Code for aerospace applications*, 50th NAL ICAST, Bangalore (India), 2008.
- [22] Spalart, P. R., Allmaras, S. R., *A one-equation turbulence model for aerodynamic flows*, AIAA Paper 92-0439, 1992.
- [23] Bechert, D.W., Stanewsky, E., Hage, W., *Windkanalmessungen an einem Transsonik-Flügel mit Strömungsbeeinflussenden Massnahmen*, DLR-IB 223-99C05, 1998.
- [24] Traub, L.W., Miller, A., Rediniotis, O., *Effects of Synthetic Jet Actuation on a Ramping NACA 0015 Airfoil*, Journal of Aircraft, V41 N5, pp 1153-1162, 2004.